Hindawi Publishing Corporation
Journal of Nanomaterials
Volume 2015, Article ID 820509, 8 pages
http://dx.doi.org/10.1155/2015/820509

Research Article

Effects of Niobium-Loading on Sulfur Dioxide Gas-Sensing Characteristics of Hydrothermally Prepared Tungsten Oxide Thick Film

Viruntachar Kruefu,[1] Anurat Wisitsoraat,[2] and Sukon Phanichphant[3]

[1]*Program in Materials Science, Faculty of Science, Maejo University, Chiang Mai 50290, Thailand*
[2]*National Electronics and Computer Technology Center, National Science and Technology Development Agency, Pathum Thani 12120, Thailand*
[3]*Materials Science Research Center, Faculty of Science, Chiang Mai University, Chiang Mai 50200, Thailand*

Correspondence should be addressed to Viruntachar Kruefu; v_viruntachar@hotmail.com

Received 7 August 2014; Revised 4 November 2014; Accepted 11 November 2014

Academic Editor: Rupesh S. Devan

Copyright © 2015 Viruntachar Kruefu et al. This is an open access article distributed under the Creative Commons Attribution License, which permits unrestricted use, distribution, and reproduction in any medium, provided the original work is properly cited.

Nb-loaded hexagonal WO_3 nanorods with 0–1.0 wt% loading levels were successfully synthesized by a simple hydrothermal and impregnation process and characterized for SO_2 sensing. Nb-loaded WO_3 sensing films were produced by spin coating on alumina substrate with interdigitated gold electrodes and annealed at 450°C for 3 h in air. Structural characterization by X-ray diffraction, high-resolution transmission electron microscopy, and Brunauer-Emmett-Teller analysis showed that spherical, oval, and rod-like Nb nanoparticles with 5–15 nm mean diameter were uniformly dispersed on hexagonal WO_3 nanorods with 50–250 nm diameter and 100 nm–5 μm length. It was found that the optimal Nb loading level of 0.5 wt% provides substantial enhancement of SO_2 response but the response became deteriorated at lower and higher loading levels. The 0.50 wt% Nb-loaded WO_3 nanorod sensing film exhibits the best SO_2 sensing performances with a high sensor response of ~10 and a short response time of ~6 seconds to 500 ppm of SO_2 at a relatively low optimal operating temperature of 250°C. Therefore, Nb loading is an effective mean to improve the SO_2 gas-sensing performances of hydrothermally prepared WO_3 nanorods.

1. Introduction

Sulfur dioxide (SO_2) is a colorless toxic gas with burning smell that causes various respiratory and cardiovascular diseases as well as environmentally hazardous acid rain [1]. There has been increasing demand for on-site monitoring of SO_2 due to rising level of SO_2 pollutant produced by various industrial processes. Presently, the concentration of SO_2 is still primarily determined by conventional techniques including gas chromatography or electrochemical detections, which are expensive, cumbersome, and impractical for on-site applications. Metal oxide semiconductor gas sensors are potential candidates for portable gas-sensing devices due to high sensitivity, good stability, low cost, small size, and simple electronic interface [1–10]. However, only few metal oxide materials including WO_3, SnO, and ZnO give significant response to SO_2 and the reported response values are still limited [1]. Among these, WO_3 exhibits relatively stable and good response to SO_2 [1, 9–13]. The gas-sensing properties towards SO_2 of WO_3-based gas sensors prepared by various methods are summarized in Table 1.

Firstly, WO_3 thick film fabricated by pyrolysis/paste casting gave an optimal response of ~12 to 800 ppm SO_2 at 400°C [9]. In addition, WO_3 sensor produced by drop casting exhibited a response of ~1.3 to 25 ppm SO_2 at a lower optimal working temperature of 200°C [10]. Similarly, WO_3 thick film sensor deposited by electrostatic spray method displayed a response of ~3 to 20 ppm SO_2 at 350°C [12]. Moreover, WO_3 sensors made by hydrothermal and screen-printing processes showed a fair response of <2 to low SO_2 concentrations of 1–10 ppm at 260°C [13]. It can be seen that undoped WO_3 sensors tend to suffer from limited SO_2 response or

Table 1: A summary of the gas-sensing properties of WO_3-based gas sensors towards SO_2.

Authors/reference	Method	Materials	Gas concentration	SO_2 sensing performances
Shimizu et al., 2001 [9]	Pyrolysis/paste casting	Unloaded WO_3	800 ppm	Response: ~12 to 800 ppm at 400°C
	Pyrolysis/impregnation/paste casting	1.0 wt% Ag/WO_3	800 ppm	Response: ~20 to 800 ppm at 450°C
Tomchenko et al., 2003 [10]	Drop casting	WO_3	25 ppm	Response: ~1.3 to 25 ppm at 200°C
Stankova et al., 2004 [11]	RF magnetron sputtering	Pt/WO_3	1 ppm	Response: ~6 to 1 ppm at 200°C, 50 μm of electrode gap
Matei Ghimbeu et al., 2010 [12]	Electrostatic spray deposition	Unloaded WO_3	20 ppm	Response: ~3 to 20 ppm at 350°C
Boudiba et al., 2012 [13]	Hydrothermal/screen-printing	WO_3 thick films	1–10 ppm	Response: <2 to 10 ppm at 260°C
This work	Hydrothermal/spin coating	0.5 wt% Nb-WO_3	25–500 ppm	Response: ~10 to 500 ppm at 250°C

high optimal working temperature. Thus, incorporations of various metallic additives including Au, Ag, Cu, Pt, Pd, and Rh have been studied to improve the SO_2 gas-sensing properties of WO_3 sensors [9, 11]. For instance, the addition of 1.00 wt% Ag to pyrolyzed WO_3 thick film sensors led to the highest response of ~20 to 800 ppm SO_2 at 450°C [9]. In another study, Pt-loaded rf-sputtered WO_3 thin film showed a good response of ~6 to 1 ppm SO_2 diluted in CO_2 at 200°C with the absence of oxygen while the response to H_2S was very low (<1), dictating good SO_2 selectivity [11]. Thus, studies of additive incorporation in WO_3 for SO_2 sensing are still limited and more effective metal additives should be explored to achieve better SO_2 gas-sensing performances.

Niobium is a noble metal catalyst that is found to be useful for gas sensing towards particular gases such as NO_2 and CO [14, 15]. However, there is no report of its addition to WO_3 support for SO_2 gas sensing. In this work, Nb nanoparticles are impregnated on WO_3 nanorods synthesized by hydrothermal synthesis and the effect of Nb loading concentration on SO_2 gas-sensing performances is studied as a function of the operating temperature and gas concentration.

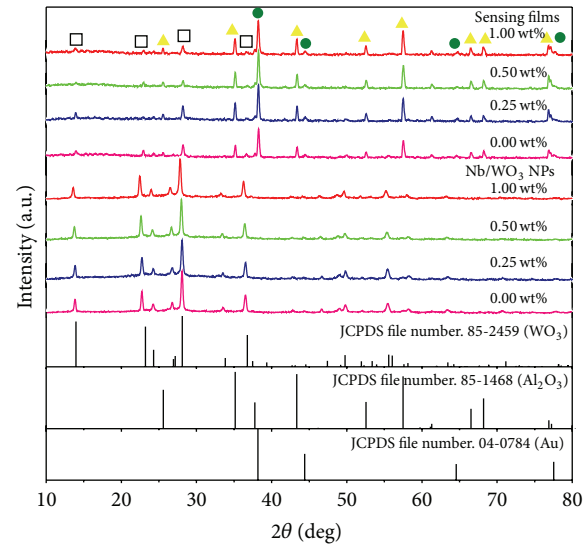

Figure 1: XRD diffraction patterns of unloaded and 0.25–1.00 wt% Nb-loaded WO_3 sensing films and powders. JCPDS files number 85-2549, 04-0784, and 82-1468 refer to (□) WO_3, (●) Au, and (△) Al_2O_3, respectively.

2. Experimental Methods

2.1. Synthesis of Material. Unloaded and Nb-loaded WO_3 nanorods were synthesized by hydrothermal and impregnation methods using sodium tungstate dihydrate ($Na_2WO_4 \cdot 2H_2O$) and sodium chloride (NaCl) as initial precursors and niobium (V) ethoxide ($Nb(OCH_2CH_3)_5$) as Nb-impregnation precursor. To synthesize unloaded WO_3 nanorods, 2.215 g of $Na_2WO_4 \cdot H_2O$ and 0.7747 g of NaCl were dissolved in 100 mL of deionized (DI) water under constant stirring. Subsequently, 3 M HCl was slowly dropped into the solution until the pH value of 2 was reached. The solution was then transferred into a Teflon-lined autoclave and the hydrothermal reaction was carried out in an oven at 100°C for 6 h. After cooling the autoclave down to room temperature, the final products were washed with DI water and ethanol several times with centrifugation. The obtained powder was subsequently dried at 60°C for 24 h in air. To impregnate Nb nanoparticles onto WO_3 nanorods, 0.0398 g of niobium (V) ethoxide was dissolved in 6 mL of methanol solution under vigorous stirring. The solution was then added to 1 g of WO_3 nanorods with Nb concentrations of 0.25, 0.50, and 1.00 wt%, respectively. The mixture was stirred until they formed smooth slurry and dried in an oven at 80°C for 2 h. Finally, the final powders were calcined at 300°C for 2 h.

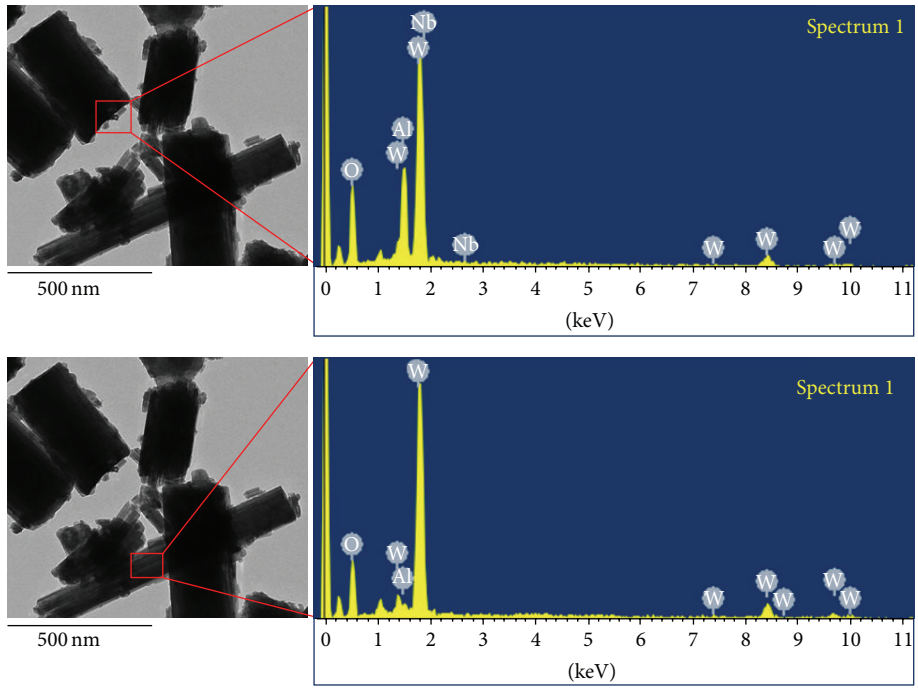

Figure 2: HRTEM bright-field images and EDX spectra of 0.5 wt% Nb-loaded WO_3 nanorods.

2.2. Material Characterization. The phase structure of unloaded WO_3 and Nb-loaded WO_3 nanorods was studied by means of X-ray diffraction (XRD; TTRAX III diffractometer, Rigaku). The morphology of nanorods was examined by high-resolution transmission electron microscopy (HRTEM; JEM-2010, JEOL). The presence of Nb element was confirmed by an energy dispersive X-ray spectroscopy (EDX). The specific surface areas (SSA_{BET}) and pore sizes of nanorods were determined from Brunauer-Emmett-Teller (BET) and Barrett-Joyner-Halenda (BJH) analyses of nitrogen adsorption measurements.

2.3. Sensing Film Fabrication and Characterization. To form paste for spin coating of sensing films, 60 mg of unloaded WO_3 or 0.25–1.00 wt% Nb-loaded WO_3 nanopowder was thoroughly mixed with an organic paste composed of ethyl cellulose and terpineol (0.25 mL), which acted as a vehicle binder and solvent, respectively. The resulting paste was spin-coated on alumina substrates equipped with interdigitated gold electrodes and then annealed at 450°C for 2 h with a heating rate of 2°C/min for binder removal. After annealing and sensing test at 350°C in dry air, the morphologies, cross section, and elemental compositions of sensing films were analyzed by glancing-incident XRD (GIXRD; TTRAX III diffractometer, Rigaku), scanning electron microscopy (SEM; JEOL JSM-6335F), and EDX spectroscopy.

2.4. Gas-Sensing Measurement. For gas-sensing measurements, unloaded and Nb-loaded WO_3 sensors were heated by the external NiCr heater to the operating temperatures ranging from 200 to 350°C in dry air before exposure to target gases in a stainless steel chamber (the setup is reported in our previous work [14]). The target gas source (1000 ppm SO_2 balanced in dry air) was flowed to mix with dry air at different flow rates to attain desired concentrations using multichannel mass flow controllers (Brook Instrument). The resistances of various sensors were continuously monitored with a computer-controlled system by voltage-amperometric technique with 10 V dc bias and current measurement through a 6487 Keithley picoammeter. The gas-sensing properties of unloaded and Nb-loaded WO_3 sensors are characterized in terms of response and response time as a function of gas concentration and operating temperature. The gas-sensing response (S) is given by $S = R_a/R_g$, where R_a and R_g are the electrical resistances of the sensor measured in the presence of pure dry air and reducing gas, respectively. The response time (T_{res}) is the time required to reach 90% of the response signal while the recovery time (T_{rec}) is the time needed to recover 90% of the baseline signal.

3. Results and Discussion

3.1. Particle and Sensing Film Characterization. The crystal structures of unloaded and 0.25–1.00 wt% Nb-loaded WO_3 nanorods and sensing films after annealing and sensing test were studied by XRD using CuK_α radiation at $2\theta = 10$–80° with a step size of 0.06° and a scanning speed of 0.72°/min as presented in Figure 1. It is seen that unloaded and Nb-loaded WO_3 nanorods prepared by hydrothermal and impregnation methods exhibit sharp XRD peaks whose locations are well matched to JCPDS 85-2459 [13], indicating polycrystalline structure of hexagonal WO_3 phase with high crystallinity. In addition, Nb diffraction peaks cannot be observed in all samples since the amount and size of Nb nanoparticles

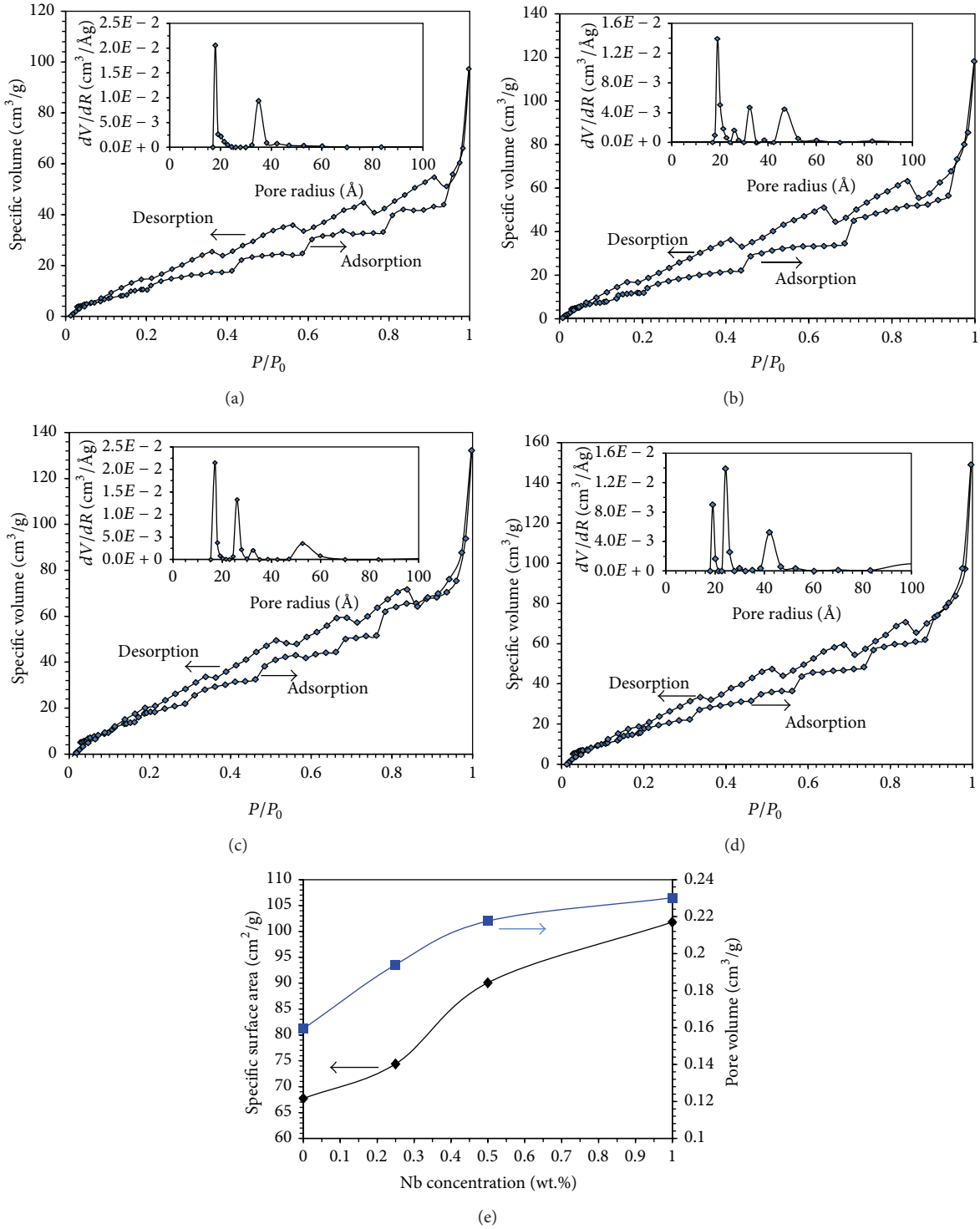

Figure 3: Nitrogen adsorption isotherm and BJH pore size distribution (inset) of (a) unloaded WO_3 nanorods, (b) 0.25 wt% Nb-loaded WO_3 nanorods, (c) 0.5 wt% Nb-loaded WO_3 nanorods, (d) 1.0 wt% Nb-loaded WO_3 nanorods, and (e) pore volume and specific surface area (SSA_{BET}) of unloaded and 0.25–1.0 wt% Nb-loaded WO_3 nanorods.

are below the detection limit of XRD instrument. Thus, the presence of Nb nanoparticles in the composite will be confirmed by HRTEM and EDS analysis. For sensing films coated on Au/Al_2O_3 substrates, the XRD patterns affirm the presence of hexagonal WO_3 phase whose diffraction peaks are weaker than those of (●) Au (JCPDS file number 04-0784 [16]) and (△) Al_2O_3 (JCPDS file number 82-1468 [17]) from the substrate.

HRTEM bright-field images and EDX spectra of 0.50 wt% Nb-loaded WO_3 nanorods synthesized by hydrothermal/impregnation are shown in Figure 2. The images show longitudinal sides of solid nanorods displaying rectangular shapes with length varying from 100 nm to 5 μm and width (the diameter of nanorod) ranging from 50 to 250 nm. In addition, the bigger nanorod surfaces are uniformly decorated with smaller spherical, oval, and rod-like nanoparticles. The mean diameter of particles is estimated to be in the range of 5–15 nm for 0.50 wt% Nb-loaded WO_3 nanorods. The EDX spectra at the two regions (Figure 2) confirm that the nanorods and nanoparticles are made of WO_3 and Nb, respectively.

The nitrogen adsorption isotherm and BJH adsorption pore size distribution (inset) of WO_3 nanorods with 0-1 wt% Nb loading levels are shown in Figures 3(a)–3(d), respectively. It can be seen that all the isotherms exhibit the IUPAC type VI pattern, indicating the existence of stepwise multilayer adsorption on nonuniform surface of nonporous adsorbent or micropores filled with multilayer adsorbates [18, 19]. In addition, adsorbed volume tends to increase with increasing Nb loading level. The pore size distributions are in multimodal forms with 2–4 maxima depending on Nb loading. The distributions of unloaded WO_3 nanorods display two maxima at ~19 and ~36 Å while those of Nb-loaded ones exhibit three significant maxima at 18–20, 26–36, and ~44–52 Å, respectively. The results indicate the surfaces are porous and contain micropores as well as mesopores structures. In addition, the contribution of larger pores tends to increase with increasing Nb loading levels. The minor maxima and minima are expected to be artifacts induced by the modeling technique. Figure 3(e) displays the corresponding pore volume and BET specific surface areas (SSA_{BET}) of WO_3 nanorods. As the Nb concentration increases from 0 to 1.00 wt%, pore volume and SSA_{BET} monotonically increase from 0.16 to 0.23 cm^3/g and from 67.72 to 101.8 m^2/g, respectively. The increased pore volume and specific surface area may be attributed to wider pore distribution due to interaction between Nb nanoparticles and WO_3 nanorods as well as increasing contribution of smaller Nb nanoparticles with increasing Nb loading level.

The typical cross-sectional SEM micrograph of 0.50 wt% Nb-loaded WO_3 film layer on an Al_2O_3 substrate equipped with interdigitated Au electrodes after the sensing test is shown in Figure 4. It is seen that the sensing film with an average thickness of ~10 μm contains loosely agglomerated nanorods. The detailed top surface morphology of nanorods is also shown in the inset. It shows that nanorods up to several microns long are slackly entangled with each other leaving many large and small pores in the film. The observed morphology indicates that the final sensing film has a large specific surface area, which should be highly beneficial for gas-sensing applications.

3.2. Gas-Sensing Properties. The changes of resistance of WO_3 nanorods with different Nb loading concentrations exposed to SO_2 pulses at various concentrations (500–20 ppm) are shown in Figure 5. It is evident that the resistance of all WO_3 sensors rapidly increases upon exposure to

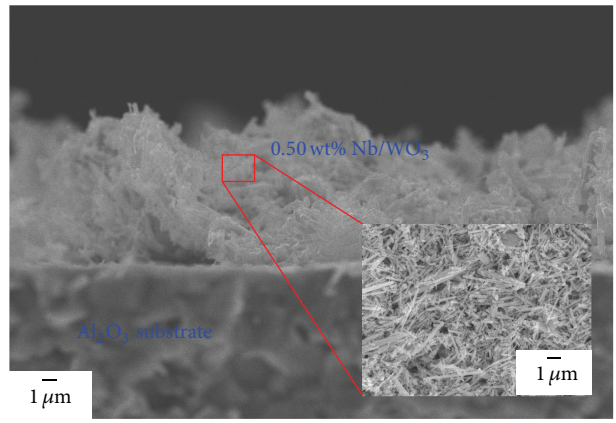

Figure 4: Cross-sectional SEM image of 0.5 wt% Nb-loaded WO_3 film on Au/Al_2O_3 substrate. Inset top-view surface morphology.

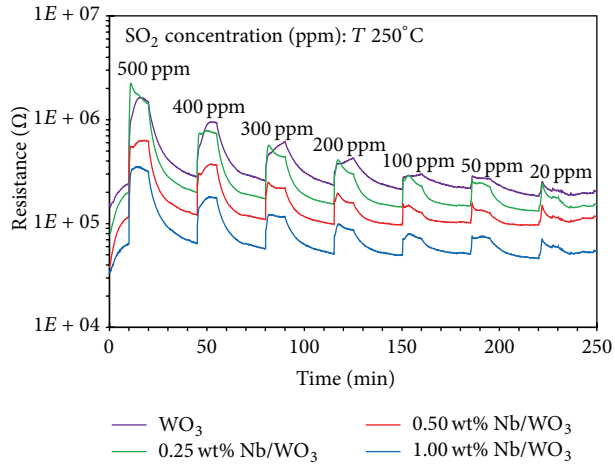

Figure 5: Change in resistance of unloaded and 0.25–1.0 wt% Nb-loaded WO_3 gas sensors to SO_2 pulses with concentration ranging from 20 to 500 ppm at 250°C.

SO_2, indicating n-type semiconducting behavior towards oxidizing gas. The result is in agreement with previous reports on SO_2 gas-sensing studies of WO_3 sensors [9, 10]. When the WO_3 nanorods are exposed to SO_2 gas, SO_2 gas will adsorb on WO_3 surface at different sites from the existing chemisorbed O_2^-, O^-, and O^{2-} ions and extract additional electrons from conduction band of WO_3 to become SO_2^- according to (1) [10]. As a result, the concentration of electrons on the surface of WO_3 nanorods decreases and the resistance of WO_3 layer increases. Consider

$$SO_2 + e^- \longrightarrow SO_2^- \text{ (ads)} \quad (1)$$

Figures 6(a) and 6(b) show the response and response time of WO_3 nanorods with different Nb loading levels versus SO_2 concentration in the range of 20–500 ppm at the operating temperature of 250°C. It can be seen that the gas-sensing behaviors of WO_3 nanorods considerably depend on Nb loading level. As the Nb loading level increases from 0 to 0.25 wt%, the SO_2 response slightly decreases but then

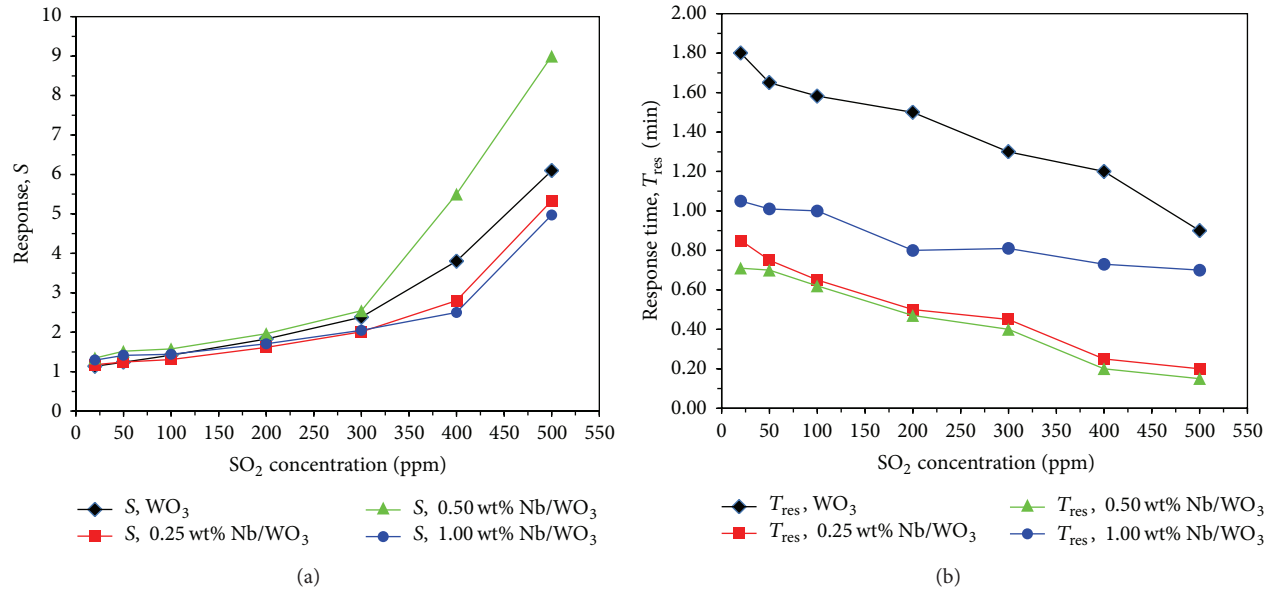

FIGURE 6: Variation of (a) response and (b) response times of unloaded and 0.25–1.0 wt% Nb-loaded WO_3 sensors versus SO_2 concentration at 250°C.

becomes significantly higher as the loading concentration increases further to 0.5 wt%. Conversely, the response time monotonically reduces as the Nb loading concentration increases from 0 to 0.5 wt%. The sensing film with 0.50 wt% Nb-loaded WO_3 nanorods exhibits the best SO_2 sensing performances with a high sensor response of ~10 and a short response time of ~6 seconds to 500 ppm of SO_2 at 250°C. Thus, the moderate Nb loading level of 0.5 wt% could substantially improve the response towards SO_2. However, the response and response time are considerably degraded when the Nb loading concentration further increases to 1.0 wt%. Regarding the baseline recovery, unloaded and Nb-loaded WO_3 nanorods have similarly long recovery times on the order of several minutes, which are not practical for gas-sensing applications. The recovery time is dictated by the sensor's inherent oxygen readsorption rate as well as gas flow dynamic. In this case, the slow gas flow dynamic due to large volume of gas-testing chamber (~3 liters) was found to be the main cause of slow recovery and the problem may be solved by miniaturization of sensors and test system.

From the results, the optimum Nb loading concentration of WO_3 nanorods for SO_2 sensing is 0.5 wt%. A possible explanation for the enhanced SO_2 response due to moderate Nb doping is that Nb nanoparticles may provide catalytic effect to enhance SO_2^- adsorption on WO_3 surface and this mechanism will be effective when there is a sufficient amount of Nb nanoparticles well dispersed on WO_3 nanorods so that electron transfer due to SO_2 adsorption can dominate the resistance control at most contacts. Moreover, Nb loading results in increased pore volume and specific surface area for gas adsorption. When the Nb loading level (i.e., 0.25 wt%) is too low, the enhancement effect is very low and the observed small response decrease may be due to the slight reduction in porosity and thickness of the final sensing film. At too high Nb loading concentration, Nb nanoparticles may become agglomerated into larger particles so that the catalytic mechanism is less effective, leading to deteriorated SO_2 response. In addition, the proposed catalytic effect may be supported by the observed significant decrease of response time with Nb loading since this effect should result in higher adsorption rate and more rapid change in resistance upon SO_2 exposure.

Figure 7 shows the effect of operating temperature on response to 500 ppm SO_2 of WO_3 nanorods with different Nb loading concentrations. It is clear that all sensors exhibit similar temperature dependence of response with optimal operating temperature of 250°C and much lower response at lower (200°C) and higher (300–350°C) temperatures. At low temperature, SO_2^- adsorption rate and SO_2 response are low due to low thermal energy. In the case of high temperature, the SO_2^- adsorption rate and response become low despite the increase of thermal energy because there is less available site for SO_2^- adsorption due to the increased concentration of preadsorbed oxygen species. The attained optimal SO_2 response (~10 to 500 ppm SO_2) and operating temperature (250°C) are relatively advantageous compared with some previously reported WO_3 sensors as listed in Table 1 that showed lower response at similar operating temperature or exhibited higher response at low concentration but required higher optimal operating temperature of 350–450°C [8–12]. However, the performances of Nb-loaded WO_3 sensor are inferior to those of Pt/WO_3 sensor that can achieve both high response and low operating temperature but the sensor requires much more expensive Pt catalyst [11]. Therefore, Nb-loaded WO_3 nanorods are a promising alternative for SO_2 sensing.

4. Conclusions

Unloaded and 0.25–1.0 wt% Nb-loaded WO_3 nanorods were successfully synthesized by hydrothermal and impregnation

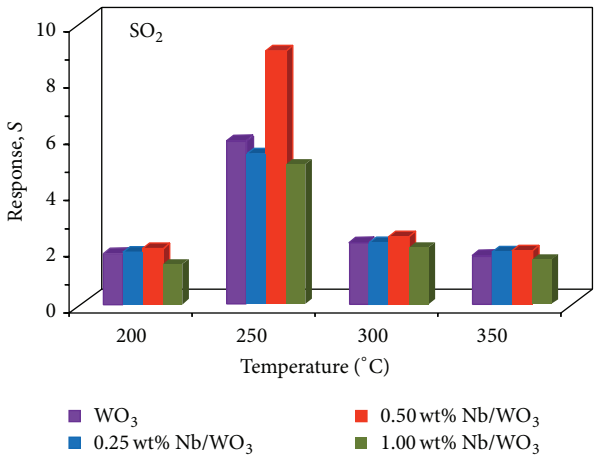

Figure 7: The response of 0.50 wt% Nb-loaded WO_3-based gas sensor towards 500 ppm SO_2 versus operating temperature.

methods. From structural characterizations, spherical, oval, and rod-like Nb nanoparticles with 5–15 nm mean diameter were uniformly dispersed on hexagonal WO_3 nanorods with 50–250 nm diameter and 100 nm–5 μm length. From gas-sensing measurement, Nb loading with the moderate level of 0.5 wt% led to substantial enhancement of SO_2 response but the response became deteriorated at lower and higher loading levels. The 0.50 wt% Nb-loaded WO_3 nanorod sensing film exhibited the best SO_2 sensing performances with a high sensor response of ~10 and a short response time of ~ 6 seconds to 500 ppm of SO_2 at a relatively low optimal operating temperature of 250°C. The enhanced SO_2 sensing performances may be attributed to catalytic effect of well dispersed Nb nanoparticles on WO_3 nanorods. Therefore, Nb loading is an effective method to enhance the SO_2 gas-sensing performances of hydrothermally prepared WO_3 nanorods.

Conflict of Interests

The authors declare that there is no conflict of interests regarding the publication of this paper.

Acknowledgments

The authors gratefully acknowledge the financial support from the National Research Council of Thailand (NRCT); Program in Materials Science, Faculty of Science, Maejo University, Thailand; the National Research University Project under Thailand's Office of the Higher Education Commission; the Graduate School and Department of Chemistry, Faculty of Science, Chiang Mai University, Thailand, and National Electronics and Computer Technology Center, Pathumthani, Thailand, are gratefully acknowledged.

References

[1] K. Wetchakun, T. Samerjai, N. Tamaekong et al., "Semiconducting metal oxides as sensors for environmentally hazardous gases," *Sensors and Actuators B: Chemical*, vol. 160, no. 1, pp. 580–591, 2011.

[2] R. S. Devan, R. A. Patil, J.-H. Lin, and Y.-R. Ma, "One-dimensional metal-oxide nanostructures: recent developments in synthesis, characterization, and applications," *Advanced Functional Materials*, vol. 22, no. 16, pp. 3326–3370, 2012.

[3] H. Zhang, S. Wang, Y. Wang, J. Yang, X. Gao, and L. Wang, "TiO_2(B) nanoparticle-functionalized WO_3 nanorods with enhanced gas sensing properties," *Physical Chemistry Chemical Physics*, vol. 16, no. 22, pp. 10830–10836, 2014.

[4] W. Zeng, C. Dong, B. Miao et al., "Preparation, characterization and gas sensing properties of sub-micron porous WO_3 spheres," *Materials Letters*, vol. 117, pp. 41–44, 2014.

[5] J. S. Lee, O. S. Kwon, D. H. Shin, and J. Jang, "WO_3 nanonodule-decorated hybrid carbon nanofibers for NO_2 gas sensor application," *Journal of Materials Chemistry A*, vol. 1, no. 32, pp. 9099–9106, 2013.

[6] S. Bai, K. Zhang, R. Luo, D. Li, A. Chen, and C. C. Liu, "Low-temperature hydrothermal synthesis of WO_3 nanorods and their sensing properties for NO_2," *Journal of Materials Chemistry*, vol. 22, no. 25, pp. 12643–12650, 2012.

[7] F. Chávez, G. F. Pérez-Sánchez, O. Goiz et al., "Sensing performance of palladium-functionalized WO_3 nanowires by a drop-casting method," *Applied Surface Science*, vol. 275, pp. 28–35, 2013.

[8] X. Su, Y. Li, J. Jian, and J. Wang, "*In situ* etching WO_3 nanoplates: hydrothermal synthesis, photoluminescence and gas sensor properties," *Materials Research Bulletin*, vol. 45, no. 12, pp. 1960–1963, 2010.

[9] Y. Shimizu, N. Matsunaga, T. Hyodo, and M. Egashira, "Improvement of SO_2 sensing properties of WO_3 by noble metal loading," *Sensors and Actuators, B: Chemical*, vol. 77, no. 1-2, pp. 35–40, 2001.

[10] A. A. Tomchenko, G. P. Harmer, B. T. Marquis, and J. W. Allen, "Semiconducting metal oxide sensor array for the selective detection of combustion gases," *Sensors and Actuators, B: Chemical*, vol. 93, no. 1-3, pp. 126–134, 2003.

[11] M. Stankova, X. Vilanova, J. Calderer et al., "Detection of SO_2 and H_2S in CO_2 stream by means of WO_3-based micro-hotplate sensors," *Sensors and Actuators B: Chemical*, vol. 102, no. 2, pp. 219–225, 2004.

[12] C. Matei Ghimbeu, M. Lumbreras, M. Siadat, and J. Schoonman, "Detection of H_2S, SO_2, and NO_2 using electrostatic sprayed tungsten oxide films," *Materials Science in Semiconductor Processing*, vol. 13, no. 1, pp. 1–8, 2010.

[13] A. Boudiba, C. Zhang, C. Bittencourt et al., "SO_2 gas sensors based on WO_3 nanostructures with different morphologies," *Procedia Engineering*, vol. 47, pp. 1033–1036, 2012.

[14] V. Kruefu, C. Liewhiran, A. Wisitsoraat, and S. Phanichphant, "Selectivity of flame-spray-made Nb/ZnO thick films towards NO_2 gas," *Sensors and Actuators, B: Chemical*, vol. 156, no. 1, pp. 360–367, 2011.

[15] A. Teleki, N. Bjelobrk, and S. E. Pratsinis, "Flame-made Nb- and Cu-doped TiO_2 sensors for CO and ethanol," *Sensors and Actuators, B: Chemical*, vol. 130, no. 1, pp. 449–457, 2008.

[16] W. Wong-Ng, H. F. McMurdie, C. R. Hubbard, and A. D. Mighell, "JCPDS-ICDD research associate ship (Cooperative program with NBS/NIST)," *Journal of Research of the National Institute of Standards and Technology*, vol. 106, no. 6, pp. 1013–1028, 2001.

[17] H. Sawada, "Residual electron density study of α-aluminum oxide through refinement of experimental atomic scattering factors," *Materials Research Bulletin*, vol. 29, no. 2, pp. 127–133, 1994.

[18] J. H. de Boer, B. C. Lippens, B. G. Linsen, J. C. P. Broekhoff, A. van den Heuvel, and T. J. Osinga, "The t-curve of multimolecular N_2-adsorption," *Journal of Colloid And Interface Science*, vol. 21, no. 4, pp. 405–414, 1966.

[19] K. S. W. Sing, D. H. Everett, R. A. W. Haul et al., "Reporting physisorption data for gas/solid systems with special reference to the determination of surface area and porosity (Recommendations 1984)," *Pure and Applied Chemistry*, vol. 57, pp. 603–619, 1985.

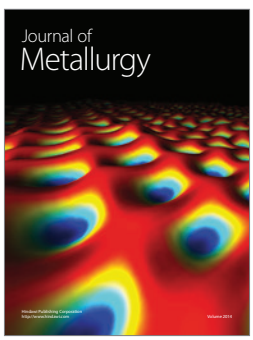

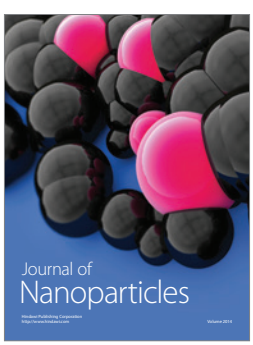

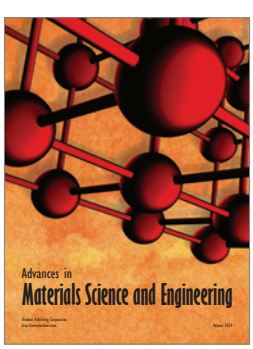

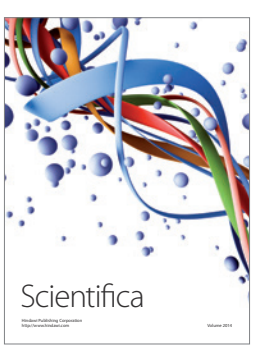

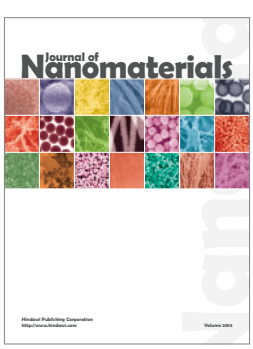

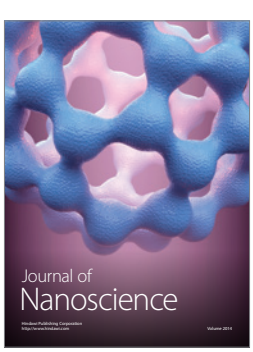

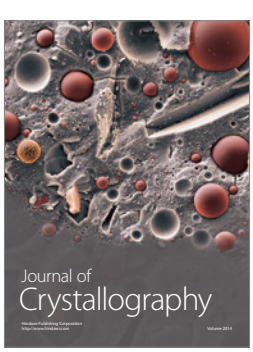

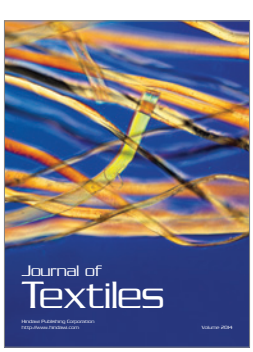

Hindawi

Submit your manuscripts at
http://www.hindawi.com